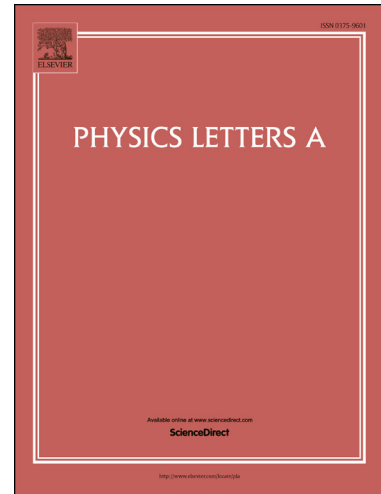


Accepted Manuscript

Effects of sm substitution on ferroelectric domains and conductivity in bismuth ferrite ceramics

Panithan Sriboriboon, Benjaporn Yotburut, Oradee Srikimkaew, Sartanee Suebka,
Arreerat Jiamprasertboon et al.

PII: S0375-9601(19)30154-9
DOI: <https://doi.org/10.1016/j.physleta.2019.02.021>
Reference: PLA 25569



To appear in: *Physics Letters A*

Received date: 22 December 2018
Revised date: 12 February 2019
Accepted date: 14 February 2019

Please cite this article in press as: P. Sriboriboon et al., Effects of sm substitution on ferroelectric domains and conductivity in bismuth ferrite ceramics, *Phys. Lett. A* (2019), <https://doi.org/10.1016/j.physleta.2019.02.021>

This is a PDF file of an unedited manuscript that has been accepted for publication. As a service to our customers we are providing this early version of the manuscript. The manuscript will undergo copyediting, typesetting, and review of the resulting proof before it is published in its final form. Please note that during the production process errors may be discovered which could affect the content, and all legal disclaimers that apply to the journal pertain.

Graphical abstract

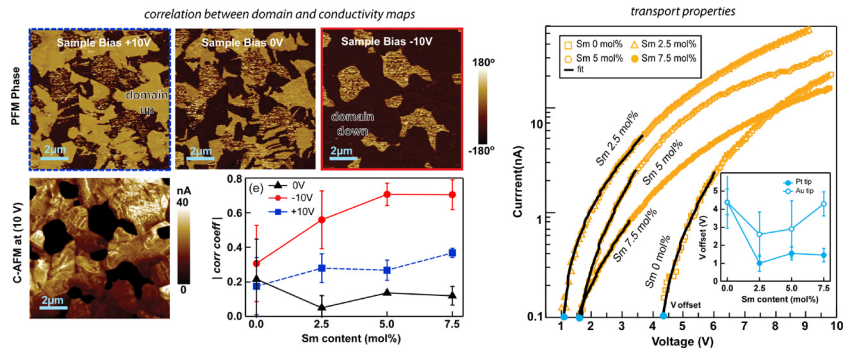
Effects of sm substitution on ferroelectric domains and conductivity in bismuth ferrite ceramics

Physics Letters A •••, •••, •••

Panithan Sriboriboon^a, Benjaporn Yotburut^a, Oradee Srikimkaew^a, Sartanee Suebka^a, Arreerat Jiamprasertboon^b, Santi Maensiri^a, Worasom Kundhikanjana^{a,*}

^a School of Physics, Institute of Science, Suranaree University of Technology, Nakhon Ratchasima, 30000, Thailand

^b School of Chemistry, Institute of Science, Suranaree University of Technology, Nakhon Ratchasima, 30000, Thailand



Highlights

- Visualization with combined piezoresponse and conductive atomic force microscopy.
- Sm-doped bismuth ferrite ceramic with phase transition at Sm 15%, no piezoresponse.
- Finite conductivity at Sm < 7.5% with surface p-type and bulk n-type.
- Small Sm-substitution increases leakage because of more conductive domain walls.
- Possible solar-cell applications.

Effects of Sm Substitution on Ferroelectric Domains and Conductivity in Bismuth Ferrite Ceramics

Panithan Sriboriboon¹, Benjaporn Yotburut¹, Oradee Srikimkaew¹, Sartanee Suebka¹, Arreerat Jiamprasertboon², Santi Maensiri¹ and Worasom Kundhikanjana¹

¹*School of Physics, Institute of Science, Suranaree University of Technology, Nakhon Ratchasima, 30000, Thailand*

²*School of Chemistry, Institute of Science, Suranaree University of Technology, Nakhon Ratchasima, 30000, Thailand*

Corresponding Author: worasom@g.sut.ac.th

ABSTRACT:

The large piezoelectric coefficient and multiferroicity of bismuth ferrite (BFO) make it an attractive candidate for lead-free ferroelectric devices. However, large leakage currents have limited broader applications. Rare-earth substitutions in BFO have been shown to improve ferroelectric and magnetic properties. In this work, we employed piezoresponse and conductive atomic force microscopy to study ferroelectric domains in $\text{Bi}_{1-x}\text{Sm}_x\text{FeO}_3$ ($x = 0 - 0.150$) grown by the co-precipitation method. The combined piezoresponse and conductivity measurements can directly visualize the local ferroelectric domains under different sample bias. At $\text{Sm mol\%} > 7.5$, Sm-substitution effectively lowers defect-generated conductivity. At $\text{Sm mol\%} < 7.5$, conductivity increases due to conductive domain walls inside sample grains. The surfaces of these conductive samples exhibit a p-type rectifying behavior while the bulk is n-type. Our work details how the local piezoelectric properties and transport behaviors of BFO ceramics change as a function of Sm-substitution.

Keywords: bismuth ferrite, ferroelectric, piezoelectric, piezoresponse force microscopy, conductive atomic force microscopy

I. INTRODUCTION

BiFeO_3 (BFO) is an attractive candidate as a lead-free piezoelectric material due to its high remnant polarization, piezoelectric coefficient, and additional multiferroicity(1). However, a large leakage current limits a number of BFO applications. Therefore, improving BFO properties by chemical substitutions either at A- or B- sites has been of great interest. Among these works, A-site substitutions with trivalent rare-earth elements with ionic radius smaller than Bi, such as Sm^{3+} , Gd^{3+} , Dy^{3+} , and La^{3+} , have shown promising results(2–8). The chemical pressure from replacing Bi with a smaller atom causes a structural transition from rhombohedral to orthorhombic, with enhanced dielectric constant(4), piezoelectric coefficient(2,4,7,9), and remanent magnetic polarization(6) at the phase boundary. This phase boundary is called the morphotropic phase boundary, similar to what is found in lead-based ferroelectric materials(10). Furthermore, the chemical substitution also reduces the number of oxygen vacancies and Fe^{2+} ions, which are the major sources of leakage in BFO(11–13).

Studies of leakage mechanisms in ferroelectric material often rely on the interpretation of frequency dependent dielectric constant measurements(2,6,8,11). Such measurements average over the entire sample and are difficult to interpret when multiple conduction mechanisms are involved. For example, domain and domain wall conduction may both contribute to leakage. Recently, much attention has been paid to transport behavior at a metal-BFO interface(14–19), such as polarization-modulated rectification(15–17), photovoltaic effect(14,15), and ferroelectric resistive switching(16,18). These transport properties are greatly influenced by domain polarization, domain walls, impurities and chemical defects(19,20), which are altered upon chemical substitution. Studying the transport properties at the metal-BFO interface requires a direct, microscopic measurement(21–23). In this work, we study the piezoresponse and transport properties of ferroelectric domains in Sm-substituted BFO ceramics using piezoresponse force microscopy (PFM)(21–23) and conductive atomic force microscopy (C-AFM). These techniques allow direct measurements of the local piezoresponse, polarization direction, conductivity, and current-voltage (I - V) characteristics of the same ferroelectric domains(14,15,17), and correlations between these

properties. These investigations further our understanding of the effects of chemical substitution on local polarization and transport properties, which are important for device applications.

II. MATERIALS AND EXPERIMENTAL DETAILS

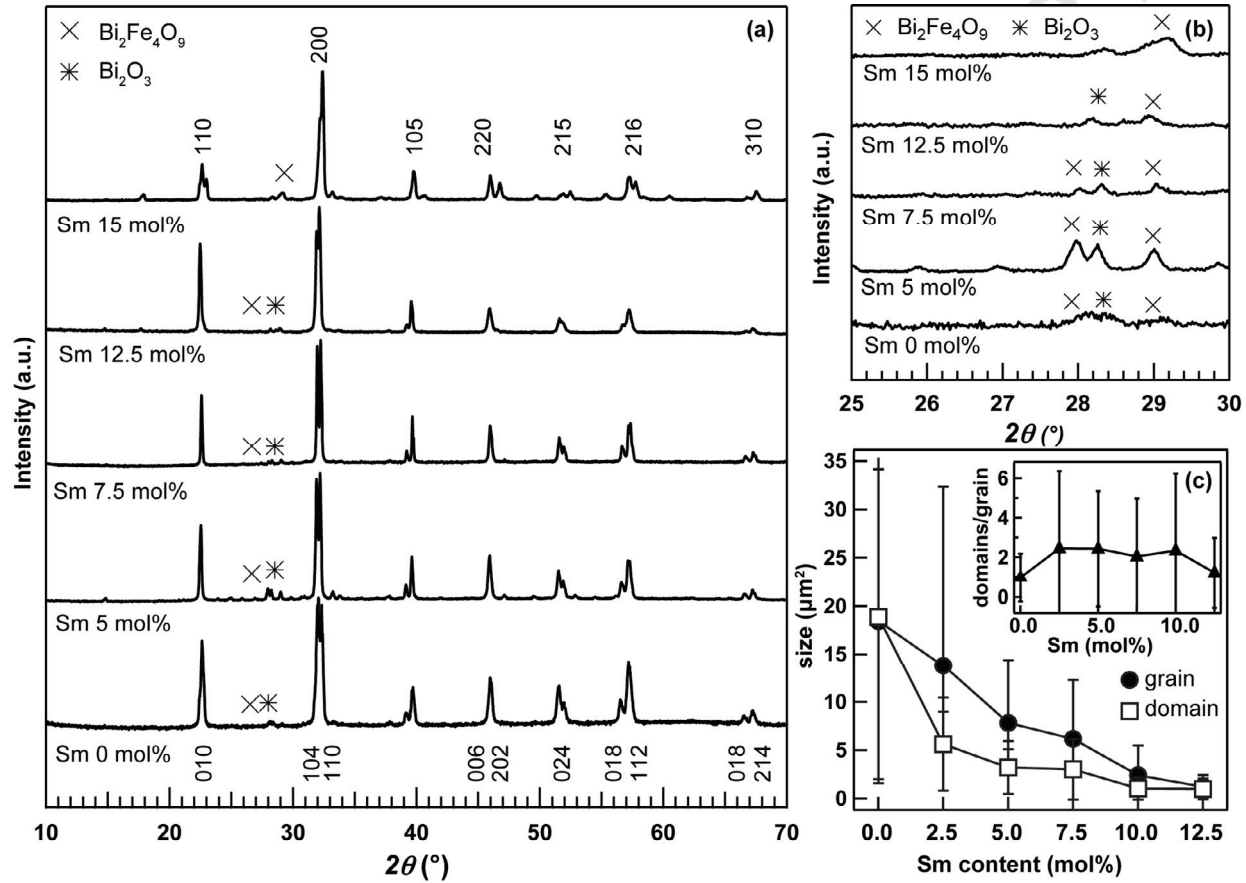


FIG.1. (a) XRD patterns of $\text{Bi}_{1-x}\text{Sm}_x\text{FeO}_3$ ($x=0, 0.025, 0.050, 0.075, 0.125, 0.150$) samples. * and \times indicate $\text{Bi}_2\text{Fe}_4\text{O}_9$ and Bi_2O_3 phases, respectively. (b) Intensity of $\text{Bi}_2\text{Fe}_4\text{O}_9$ and Bi_2O_3 phases at $2\theta=28^\circ$. (c) Weighted Average grain and ferroelectric domain size as a function of Sm-content.

Sm-substituted bismuth ferrite ($\text{Bi}_{1-x}\text{Sm}_x\text{FeO}_3$) ceramic samples with $x=0, 0.025, 0.050, 0.075, 0.100, 0.125$, and 0.150 were prepared by a simple co-precipitation method as detailed in reference(8). We first performed macroscopic characterization. The sintered ceramic samples were ground up in preparation for structure and phase

identification using x-ray diffraction (XRD) on a D2 (Bruker Corp., Ettlingen, Germany) X-ray diffractometer (voltage = 30 kV, Cu-K α) over a range of $20^\circ \leq 2\theta \leq 70^\circ$, with a step width = 0.02° . Fig 1(a) and Supplementary Material show XRD patterns of Sm-substituted BFO samples. At Sm mol% lower than 15, the samples have rhombohedral structure, and at higher substitution levels transition to orthorhombic structure, in agreement with previous studies(5,22,24). Fig 1(b) shows an enlarged view of the XRD spectrum between $2\theta = 25^\circ\text{-}30^\circ$. Secondary phases, Bi₂Fe₄O₉and Bi₂O₃, are present for all samples, but the peak intensity is the greatest in the Sm 2.5mol% and 5mol% samples(8,25). The macroscopic frequency-dependent impedance spectroscopy for various temperature can be found in reference(8).

Out-of-plane piezoelectric force microscope (PFM) and conductive atomic force microscope (C-AFM) images were taken on a commercial atomic force microscopy (XE-120 Park AFM, Park Systems Corp., Korea). Both PFM and C-AFM images were taken at the same area. The samples were not polished nor poled prior to the measurements. For the PFM measurement, we applied voltage (2.5 V, peak-to-peak at 17 kHz) to the probe using a function generator (33210A, Keysight Technologies Inc., USA), and measured the piezoresponse from the photodetector using a lock-in amplifier (SR-830, Stanford Research Systems, USA). For the C-AFM image, the current maps were measured under a constant sample bias (V_{sample}). Finally, conductive regions in the middle of the ferroelectric domains were chosen for current-voltage (I - V) curve measurements. The voltage sweep was performed at a ramp rate of 0.04 V/s. For each sample, we collected images from 5 randomly selected regions and about 150 – 200 points for the I - V curve. PFM and C-AFM imaging was conducted with solid platinum (Pt) probes with spring constant 290 N/m and resonance frequency 105 kHz (25Pt200A-H, Rocky Mountain Nanotechnology, USA). For the transport measurements, we use the Pt and gold-coated (Au) probes with spring constant 37 N/m and resonance frequency 300 kHz (ACTGG, Applied NanoStructures, USA)

Average grain and domain sizes were extracted from the AFM and PFM amplitude images using ImageJ software. We use correlation coefficient (r) to describe similarity between PFM phase and C-AFM images. We scale the C-

AFM signal to between 0 and 1. The PFM phase image signal is similarly scaled to between -1 and 1. Both images are reshaped to two one dimensional arrays (x, y) and used in the following equation:

$$r = \frac{\sum_{i=1}^n (x_i - \bar{x})(y_i - \bar{y})}{\sigma_x \sigma_y}$$

where \bar{x} and \bar{y} , σ_x and σ_y are the mean and standard deviation of x and y . For this work, positive and negative r values have the same meaning, and therefore only the absolute value of r will be shown. Calculation of the correlation coefficient and I - V curve fitting were done using custom MATLAB programs.

III. RESULTS AND DISCUSSION

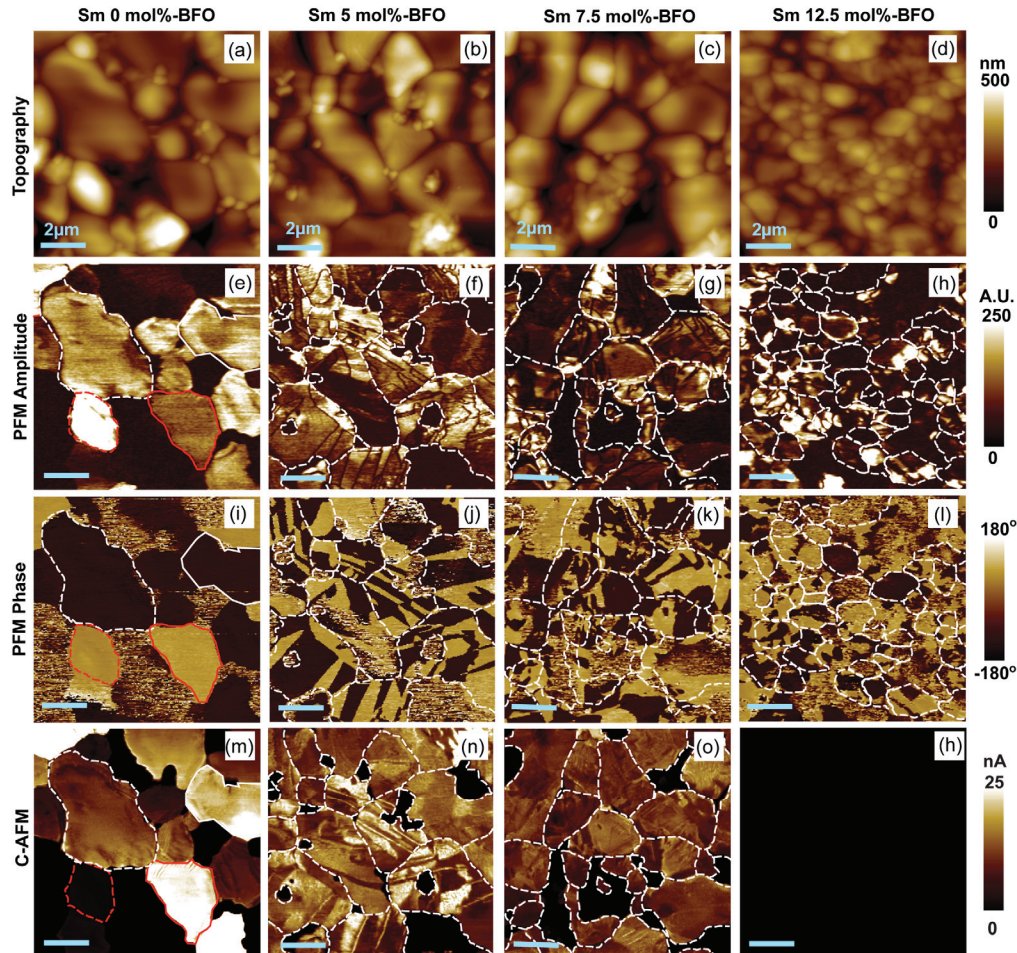


FIG.2. (color online) (a) – (d) Topography, (e)-(h) PFM amplitude, (i) – (l) PFM Phase, and (m) – (p) C-AFM images of $\text{Bi}_{1-x}\text{Sm}_x\text{FeO}_3$ ($x= 0, 0.050, 0.075$, and 0.125) samples. For Sm 0 mol% images, the red and white lines outline grains from the topography images with different PFM and C-AFM responses (see main text for details). For Sm 5 mol% -12.5 mol%, the dash lines simply outline grains from the topography images. All scale bars are 2 μm .

Fig. 2 shows AFM, PFM and C-AFM images of $\text{Bi}_{1-x}\text{Sm}_x\text{FeO}_3$ ($x= 0, 0.050, 0.075$, and 0.125) samples. Images obtained from different locations in the same sample are found in the Supplementary Material. From the AFM images, the BFO ceramics consist of grains with different sizes. A plot of the weighted average grain size for different samples is summarized in Fig. 1(c). It is clear from the image in Fig. 2(a) – 2(d) that the large grains with approximately 3 - 8 μm diameter comprise a significant volume fraction in Sm mol% < 7.5 samples. The grain size decreases as the Sm content increases. For the Sm 12.5 mol% sample, the grain size is rather uniform, at approximately 1 μm .

PFM images directly visualize the effect of Sm-substitution on ferroelectric domains in BFO. Fig. 2(e)-2(h) and 2(i)-2(l) show PFM amplitude and PFM phase images. The PFM amplitude signal is proportional to the local piezoelectric coefficient of the ferroelectric domain in the out-of-plane direction. The out-of-plane polarization direction is indicated in our PFM phase image by bright yellow, dark, and noisy regions, which represent domain up, down, and horizontal or no PFM response, respectively. For Sm 0 mol% BFO sample, the PFM responses (both amplitude and phase Fig. 2(e) and Fig. 2(i)) varies weakly as a function of position within a single grain, while in the Sm 5.0 mol% - 7.5 mol% samples (Fig. 2(f) – 2(h) and Fig. 2(j) – 2(l)), the PFM responses vary significantly within a single grain. From the PFM responses, we can calculate the area weighted average domain size (Fig. 1(c)) and number of ferroelectric domains per grain (Fig. 1(c), inset) as a function Sm-substitution. In the Sm 0 mol% sample, the ferroelectric domains are as big as the material grain size, while in the Sm 2.5 – 10 mol% samples, the domains are smaller than the grain size. Therefore, the Sm 0 mol% sample has an average of one domain per grain, and the Sm 2.5 – 10 mol% samples have about 3 domains per grain. For Sm mol% > 10,

both grain and domain size are about $1 \mu\text{m}^2$, giving about 1 domain per grain. Such domain texture within each grain in the Sm 2.5 – 10 mol% samples is likely due to the fact that the ferroelectric domains are sensitive to pressure introduced by the smaller Sm atoms, which can be seen in the shift in the XRD spectrum (Supplementary Information). At Sm 15 mol%, the PFM response vanishes (see Supplement Material for the images); this is the same point as the structural transition seen in the XRD measurements. At this Sm content, the structural transition to orthorhombic suppresses ferroelectricity, in agreement with previous studies(5).

Sm-substitution also changes the conductivity of ferroelectric domains in the BFO samples. The C-AFM images (Fig. 2(m)-2(p)) reveal the local current map of the sample with $V_{sample}= 10 \text{ V}$. The C-AFM current signal is proportional to the local conductivity of the material, despite being a mixed grain sample(26) (see Supplement Material for the equation). In the images, regions with higher/lower conductivity are indicated with bright/dark color. In the Sm 0 mol% – 5 mol% samples, each ferroelectric domain defined by the PFM phase images has the same conductivity within the domain, but the conductivity of different domains varies. At the boundary of the ferroelectric domains in the Sm 5 mol% sample, conductive domain walls(27) are also seen as bright lines in the C-AFM image (Fig. 2(n)). On average, the Sm 0 mol% – 7.5 mol% samples are conductive, but the conductivity decreases significantly at the 7.5% doping level. The Sm 12.5 mol% sample is not conductive, with average current around 1 nA, the noise level of our measurement. We note that using an opposite voltage polarity $V_{sample}= -10 \text{ V}$, gives no C-AFM signal, indicating rectification behavior, which will be discussed later.

Three major contributions to the conductivity of BFO have previously been identified: chemical defects (such as oxygen, Bi and Fe vacancies), domain walls, and grain boundaries(13). Increasing defects and domain walls increase conductivity, while increasing grain boundaries decreases conductivity. Among the three, it appears that defects are the most likely source of leakage in our samples. Consider the Sm 5% and 7.5% samples with similar grain size and amount of domain walls, as indicated by the average grain size and average domain size in Fig 1(c). If domain walls are the main contribution to conductivity, then the conductivity of these two samples should be similar. However, the 7.5% sample has significantly lower conductivity. It also has a smaller amount of secondary

phases, as seen from the lower peak intensity in its XRD spectrum. It is well known that the secondary phase occurs along with chemical defects(8,28); therefore, we deduce that Sm substitution effectively reduces the leakage in BFO samples at Sm > 7.5% because of reduced chemical defects. It is notable that at Sm 12.5 mol% substitution, just before the structural transition, the sample has large piezoresponse, but low leakage, a desirable property for piezoelectric device applications. These promising features, at the same substitution level, have been seen in earlier works (3,4,6,22,24).

Previous studies have also observed polarization-modulation effects on transport properties, where the up and down domains have different current responses(16–19,29). When looking at the PFM phase and C-AFM images of the Sm 0 mol% sample (Fig. 2(e), 2(i) and 2(m)), we observe no obvious indication of such correlation. For example, the grains marked by the white dash and white solid lines are both down domains but have different current signals. The domains in the grains marked by the red dash and red solid lines are both up domains, but only that marked by the red solid line has a current signal. Similarly, when comparing the PFM amplitude and C-AFM images, we also found no quantitative correlation between the strength of PFM amplitude response and the current signal. For example, the two domains marked by the dash lines both have high PFM response, but different C-AFM signals.

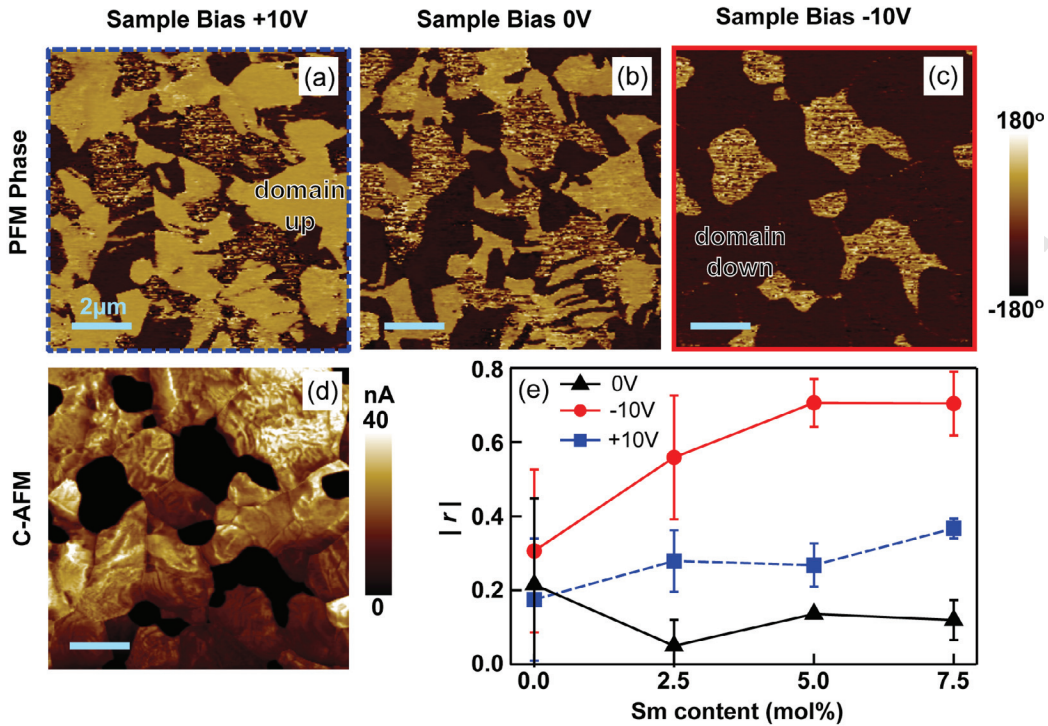


FIG.3. (a) – (c) PFM Phase image of Sm 5% sample taken at $V_{sample}=10$, 0, and -10 V. (d) C-AFM images of the same region at $V_{sample}=10$ V. (e) Absolute correlation coefficient between the C-AFM at 10 V and the PFM phase images taken at different V_{sample} as a function of Sm content. All scale bars are 2 μm .

Sample bias during the C-AFM measurement also flips the ferroelectric domains. Fig. 3(a) - 3(c) show PFM phase images taken at $V_{sample} = 10$, 0 and -10 V for the Sm 5 mol% sample. There are more up domains when applying positive bias, and more down domains when applying negative bias. Similar behaviors were seen in other Sm-substituted BFO samples with different Sm content; images for these samples can be found in the Supplementary Material. Closer inspection reveals similarity between the C-AFM image at $V_{sample} = 10$ V (Fig. 3(d)) and the PFM image at $V_{sample} = -10$ V (Fig. 3(c)). This is best captured by a correlation coefficient (r). Fig. 3(e) plots $|r|$ between the C-AFM and the PFM phase images taken at the same area for various doping. Relative to the PFM phase image at $V_{sample} = 0$ V (Fig. 3(b)), the PFM phase image at $V_{sample} = 10$ V (Fig. 3(a)) has a higher correlation with the C-AFM image (Fig. 3(d)) because it has more saturated up domains. However, the $|r|$ value

is still lower than the $|r|$ for the PFM Phase at $V_{sample} = -10$ V (Fig. 3(e)) because at $V_{sample} = -10$ V, the saturation of down domains is even more prominent.

To understand this result, we first consider the PFM phase image at $V_{sample} = 0$ V (Fig. 3(b)). The regions with noisy PFM phase signals indicate regions with no piezoresponse or domains with horizontal polarization. When applying a sample bias, domains with horizontal polarization will start to have vertical polarization. If there is no local polarization, then an applied bias will have no effect of the PFM response. These are the noisy regions in the PFM phase image at $V_{sample} = -10$ V (Fig. 3(c)). From the C-AFM image, these regions are also not conductive, and hence likely the non-ferroelectric secondary phase. Applying either positive or negative biases did not affect the PFM images of the Sm 0 mol% sample. For samples with higher Sm mol%, the PFM phase images are similar to the C-AFM images because domains flip along the applied electric field. Overall, the $|r|$ value along the $V_{sample} = -10$ V is higher than those long the $V_{sample} = 10$ V, indicating that it is easier to flip the domain downward. This observation is consistent with the p-type behavior at the surface.

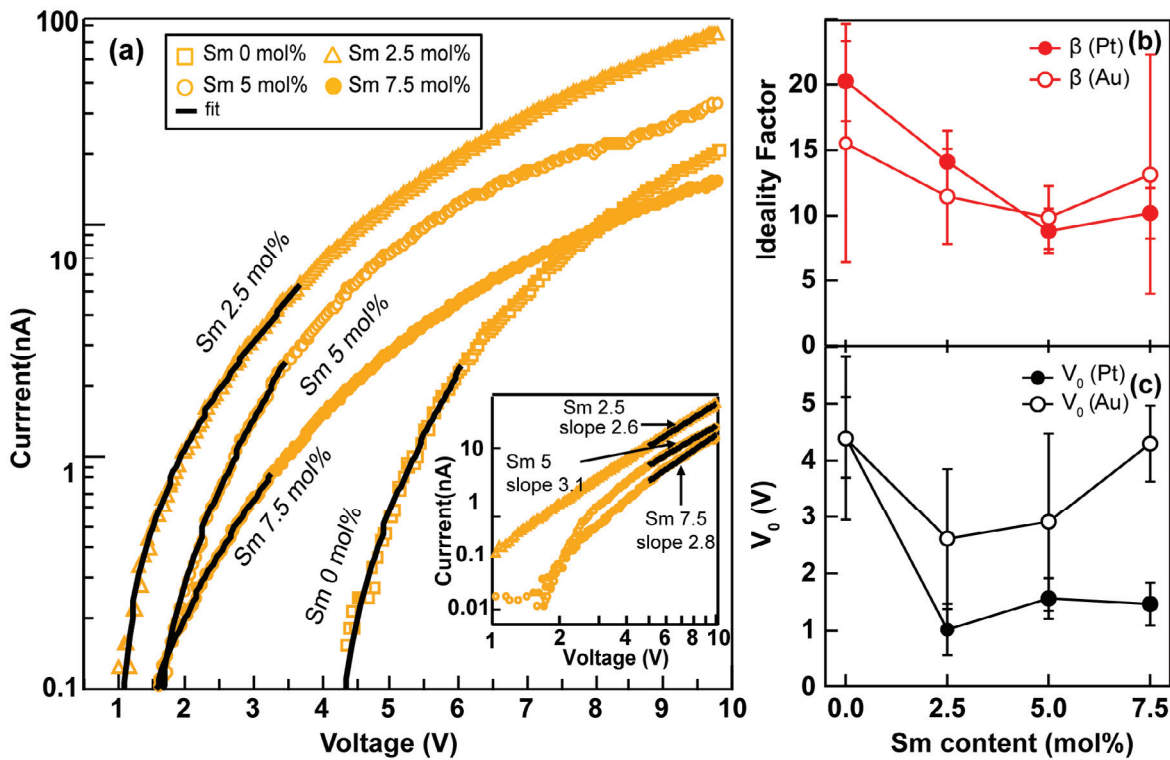


FIG.4. (a) I - V curves of ferroelectric domains $\text{Bi}_{1-x}\text{Sm}_x\text{FeO}_3$ ($x = 0 - 0.075$) in semi-logarithmic scale taken with Pt probe. The double logarithmic plot is shown in the inset. The black lines are exponential fits and linear fits, respectively. Slopes of the linear fit are indicated. (b) – (c) ideality factor (β), and offset voltages (V_0) extracted from the I - V curves as a function of Sm content from the I - V curves taken with the Pt and Au probes.

To better understand the effect of Sm-substitution on the leakage of BFO ceramics, we studied I - V characteristics of ferroelectric domains in Sm 0 – 7.5 mol% samples. Fig. 4(a) shows typical I - V curves taken with Pt probe plotted on semi-logarithmic scales. All I - V curves show rectification with the forward current when applying positive bias to V_{sample} (I - V curves during reverse bias can be found in Supplementary Materials). The I - V curves indicate p-type carriers at the tip-sample interface(15,17,18). This is different from observations in hot point probe tests and frequency-dependent measurements(8), which show a bulk n-type carrier for all samples. Similar results were obtained using a gold-coated probe (see Supplementary Information for the representative I - V curves). P-type carriers in BFO are due to the presence of Bi and Fe vacancies(20,30–32). Due to the volatile

nature of Bi ions, they may leave the surface during growth, resulting in a p-type surface layer, while the bulk remains n-type. Different carrier types at the metal-sample interface from the bulk have been observed in other ferroelectric materials(17,30).

The I - V characteristics of Sm-substituted BFO are divided into two regimes: $V_{sample} < 6$ V and $V_{sample} > 6$ V. At $V_{sample} > 6$ V, the I - V curves deviate from the diode equation and can be described by space-charge limited conduction (SCLC). Fig. 4(inset) shows double log plots of the I - V curves, which give a straight line, indicating that $I \propto V^n$. The slope of the double log plot is the power, n . We obtained $n \sim 2.6 - 3.1$. $n > 2$ behavior is referred to as trap-controlled SCLC(33), further evidence of defect-dominated transport.

At $V_{sample} < 6$ V, the current increases exponentially, suggesting a Schottky-like barrier at the tip-sample interface(18,29). The I - V curves are best describe by the Schottky diode equation $I \propto \exp(eV/\beta k_B T) - 1$, where V is the voltage at the junction, e is the electron charge, β is the ideality factor, k_B is the Boltzmann constant, and T is the temperature. Since, our I - V curves show current above the noise level at an offset voltage V_o , it is appropriate to use a reduced V , $V = V_{sample} - V_o$. We found that other models such as Poole–Frenkel emission cannot describe the measured I - V curves (see Supplementary Material for the fit results). Fig. 4(b), and 4(c) plot β , and V_o as a function of Sm-content for both Pt and Au probes. Both probes obtain the ideality factor $\beta \sim 10 - 20$, which indicates defect-dominated transport. An ideality factor much larger than 1 was found in previous studies(15,29) and were attributed to two factors: highly doped samples or defective p-n junctions(34). Since the ideality factor remains the same across different doping level, we attribute the large ideality factor to defects.

The offset voltage V_o is doping dependent. V_o depends on the work function of the metal and on the series resistance of the junction. For the Sm 0 mol% sample, $V_o = 4.5$ V. For the Sm 2.5– 7.5 mol% samples, V_o values obtained by the Pt probe are similar, in the range of 1 – 2.5 V. The offset voltage V_o obtained by the Au probes for the Sm 2.5– 7.5 mol% samples are ~ 3 – 4 V, higher than the Pt probe. This is because the work function of the Au probe is lower. The higher V_o for the Sm 0 mol% sample suggests larger series resistance to the metal-BFO

junction. This means that the bulk resistance of the BFO ceramic at Sm 0 mol% is higher than that in the Sm 2.5 – 7.5 mol% samples. These samples have similar amounts of secondary phase and defects, so the higher resistance in the Sm 0 mol% sample cannot be attributed to these two factors. Instead, we attribute the higher resistance to the lack of domain walls. From the number of ferroelectric domains per grain in Fig. 1(c) inset, the Sm 0 mol% sample has no domain wall inside the grain, while the Sm 2.5 – 7.5 mol% samples have about 3 domains per grain and multiple conductive domain walls (also seen directly from the C-AFM image in Fig. 2(n) – 2(o)). These conductive domain walls effectively lower the series resistance and V_o , leading to increased leakage in these samples.

IV. CONCLUSIONS

In summary, we performed PFM and C-AFM studies of Sm-substituted BFO ceramics, with a doping level of 0 – 15 mol%, grown by the co-precipitation method. XRD spectrums indicate a structural transition from rhombohedral to orthorhombic at Sm 15 mol% doping. The combined local PFM and C-AFM measurements can discern ferroelectric grains from non-ferroelectric ones, and enabled us to direct our investigation to conductive ferroelectric regions. As a function of Sm-substitution levels, the samples are divided into leaky (Sm-substitution < 12.5 mol% substitution) and non-leaky (Sm-substitution \geq 12.5 mol%). The leaky BFO sample surfaces exhibit p-type behavior while the bulk is n-type. In the Sm 2.5 mol% – 7.5 mol% samples, Sm-substitution increases leakage by increasing the amount of within grain, conductive domain walls, which may be an unintended and undesirable effect for ferroelectric applications, but could be useful for solar-cell applications. The amount of secondary phases and conductivity decrease in the Sm \geq 7.5 mol% samples, as seen in the XRD spectrums and C-AFM signal. As the amount of Sm-substitution increases, the sample changes from a leaky ferroelectric with defect-dominated transport properties in the Sm 2.5 – 7.5 mol% samples, to a lossless ferroelectric at Sm 12.5 mol%. Such lossless property is desirable for memory device applications.

Acknowledgments

The authors wish to thank Development and Promotion of Science and Technology Talents Project Scholarship Program, Thailand, and Center for Scientific and Technological Equipment (CSTE), Suranaree University of Technology (SUT). This project is supported by the Thailand Research Fund (TRF) <http://www.trf.or.th/> (contract number TRG5880060), Suranaree University of Technology (SUT) www.sut.ac.th, and (contract number SUT1-105-59-12-11 and SUT1-105-58-12-22), NANOTEC-SUT Center of Excellence on Advanced Functional Nanomaterials, and the Office of the Higher Education Commission under the National Research University (NRU) project.

REFERENCES

1. Catalan G, Scott JF. Physics and Applications of Bismuth Ferrite. *Adv Mater* [Internet]. 2009 Jun 26 [cited 2013 Sep 20];21(24):2463–85. Available from: <http://doi.wiley.com/10.1002/adma.200802849>
2. Fujino S, Murakami M, Anbusathaiah V, Lim SH, Nagarajan V, Fennie CJ, et al. Combinatorial discovery of a lead-free morphotropic phase boundary in a thin-film piezoelectric perovskite. *Appl Phys Lett.* 2008;92(20):12–5.
3. Kan D, Cheng CJ, Nagarajan V, Takeuchi I. Composition and temperature-induced structural evolution in La, Sm, and Dy substituted BiFeO₃ epitaxial thin films at morphotropic phase boundaries. *J Appl Phys.* 2011;110(1).
4. Cheng CJ, Kan D, Anbusathaiah V, Takeuchi I, Nagarajan V. Microstructure-electromechanical property correlations in rare-earth-substituted BiFeO₃ epitaxial thin films at morphotropic phase boundaries. *Appl Phys Lett.* 2010;97(21):10–3.
5. Khomchenko VA, Paixão JA, Shvartsman V V., Borisov P, Kleemann W, Karpinsky D V., et al. Effect of Sm substitution on ferroelectric and magnetic properties of BiFeO₃. *Scr Mater.* 2010;62(5):238–41.
6. Yuan GL, Or SW. Multiferroicity in polarized single-phase Bi_{0.875}Sm_{0.125}FeO₃ ceramics. *J Appl Phys* [Internet]. 2006;100(2):024109. Available from: <http://www.scopus.com/inward/record.url?eid=2-s2.0-33746840926&partnerID=tZOTx3y1>

7. Walker J, Simons H, Alikin DO, Turygin AP, Shur VY, Kholkin AL, et al. Dual strain mechanisms in a lead-free morphotropic phase boundary ferroelectric. *Sci Rep [Internet]*. Nature Publishing Group; 2016;6(December 2015):1–8. Available from: <http://dx.doi.org/10.1038/srep19630>
8. Yotburut B, Thongbai P, Yamwong T, Maensiri S. Synthesis and characterization of multiferroic Sm-doped BiFeO₃nano powders and their bulk dielectric properties. *J Magn Magn Mater [Internet]*. Elsevier B.V.; 2017;437:51–61. Available from: <http://dx.doi.org/10.1016/j.jmmm.2017.04.041>
9. Kan D, Palova L, Anbusathaiah V, Cheng CJ, Fujino S, Nagarajan V, et al. Universal behavior and electric-field-induced structural transition in rare-earth-substituted BiFeO₃. *Adv Funct Mater*. 2010;20(7):1108–15.
10. A. Ibrahim A-BM, Murgan R, Abd Rahman MK, Osm J, Ibrahim A-BMA. Morphotropic Phase Boundary in Ferroelectric Materials. In: Murgan R, editor. *Ferroelectrics - Physical Effects [Internet]*. Rijeka: IntechOpen; 2011. p. Ch. 1. Available from: <https://doi.org/10.5772/17206>
11. Mishra RK, Pradhan DK, Choudhary RNP, Banerjee A. Effect of yttrium on improvement of dielectric properties and magnetic switching behavior in BiFeO₃. *J Phys Condens Matter*. 2008;20(4).
12. Coondoo I, Panwar N, Bdikin I, Puli VS, Katiyar RS, Kholkin AL. Structural, morphological and piezoresponse studies of Pr and Sc co-substituted {BiFeO}3ceramics. *J Phys D Appl Phys [Internet]*. {IOP} Publishing; 2012 Jan;45(5):55302. Available from: <http://dx.doi.org/10.1088/0022-3727/45/5/055302>
13. Makhdoom AR, Akhtar MJ, Rafiq MA, Hassan MM. Investigation of transport behavior in Ba doped BiFeO₃. *Ceram Int*. 2012;38(5):3829–34.
14. Paillard C, Bai X, Infante IC, Guennou M, Geneste G, Alexe M, et al. Photovoltaics with Ferroelectrics: Current Status and Beyond. *Adv Mater*. 2016;28(26):5153–68.
15. Choi T, Lee S, Choi YJ, Kiryukhin V, Cheong SW. Switchable ferroelectric diode and photovoltaic effect in BiFeO₃. *Science (80-)*. 2009;324(5923):63–6.
16. Wang C, Jin KJ, Xu ZT, Wang L, Ge C, Lu H Bin, et al. Switchable diode effect and ferroelectric resistive switching in epitaxial BiFeO₃thin films. *Appl Phys Lett*. 2011;98(19).

17. Lee D, Baek SH, Kim TH, Yoon JG, Folkman CM, Eom CB, et al. Polarity control of carrier injection at ferroelectric/metal interfaces for electrically switchable diode and photovoltaic effects. *Phys Rev B - Condens Matter Mater Phys.* 2011;84(12):1–9.
18. Miranda E, Jiménez D, Tsurumaki-Fukuchi A, Blasco J, Yamada H, Suñé J, et al. Modeling of hysteretic Schottky diode-like conduction in Pt/BiFeO₃/SrRuO₃ switches. *Appl Phys Lett.* 2014;105(8):0–4.
19. Kim TH, Jeon BC, Min T, Yang SM, Lee D, Kim YS, et al. Continuous control of charge transport in Bi-Deficient BiFeO₃films through local ferroelectric switching. *Adv Funct Mater.* 2012;22(23):4962–8.
20. Yang CH, Seidel J, Kim SY, Rossen PB, Yu P, Gajek M, et al. Electric modulation of conduction in multiferroic Ca-doped BiFeO₃ films. *Nat Mater.* 2009;8(6):485–93.
21. Soergel E. Piezoresponse force microscopy (PFM). *J Phys D Appl Phys [Internet].* 2011;44(46):464003. Available from: <http://stacks.iop.org/0022-3727/44/i=46/a=464003>
22. Alikin DO, Turygin a. P, Walker J, Rojac T, Shvartsman V V., Shur VY, et al. Quantitative phase separation in multiferroic Bi0.88Sm0.12FeO₃ ceramics via piezoresponse force microscopy. *J Appl Phys [Internet].* 2015;118(7):072004. Available from: <http://scitation.aip.org/content/aip/journal/jap/118/7/10.1063/1.4927812>
23. Kholkin AL, Shvartsman V V, Kiselev DA, Bdikin IK. Nanoscale Characterization of Ferroelectric Materials for Piezoelectric Applications. *Ferroelectrics [Internet].* Taylor & Francis; 2006 Oct 1;341(1):3–19. Available from: <https://doi.org/10.1080/00150190600889304>
24. Khomchenko VA, Paixão JA, Costa BFO, Karpinsky D V., Kholkin AL, Troyanchuk IO, et al. Structural, ferroelectric and magnetic properties of Bi0.85Sm0.15FeO₃ perovskite. *Cryst Res Technol [Internet].* 2011;46(3):238–42. Available from: <http://doi.wiley.com/10.1002/crat.201100040>
25. Yang H, Dai J, Wang L, Lin Y, Wang F, Kang P. A novel approach to prepare Bi₂Fe₄O₉ flower-like spheres with enhanced photocatalytic performance. *Sci Rep. Springer US;* 2017;7(1):768.
26. Kalinin S V., Gruverman A. Scanning Probe Microscopy (2 vol. set): Electrical and Electromechanical Phenomena at the Nanoscale. *Scanning Probe Microscopy : Electrical and Electromechanical Phenomena at the Nanoscale.* 1st ed. Springer;

27. Seidel J, Martin LW, He Q, Zhan Q, Chu Y-H, Rother a, et al. Conduction at domain walls in oxide multiferroics. *Nat Mater.* 2009;8(3):229–34.
28. Coondoo I, Panwar N, Bdikin I, Puli VS, Katiyar RS, Kholkin AL. Structural, morphological and piezoresponse studies of Pr and Sc co-substituted BiFeO₃ ceramics. *J Phys D Appl Phys* [Internet]. {IOP} Publishing; 2012 Jan;45(5):55302. Available from: <http://stacks.iop.org/0022-3727/45/i=5/a=055302>
29. Wu W, Guest JR, Horibe Y, Park S, Choi T, Cheong SW, et al. Polarization-modulated rectification at ferroelectric surfaces. *Phys Rev Lett.* 2010;104(21):1–4.
30. Pintilie L, Alexe M. Metal-ferroelectric-metal heterostructures with Schottky contacts. I. Influence of the ferroelectric properties. *J Appl Phys.* 2005;98(12).
31. Zhang Z, Wu P, Chen L, Wang J. Density functional theory plus U study of vacancy formations in bismuth ferrite. *Appl Phys Lett.* 2010;96(23):2008–11.
32. Paudel TR, Jaswal SS, Tsymbal EY. Intrinsic defects in multiferroic BiFeO₃ and their effect on magnetism. *Phys Rev B - Condens Matter Mater Phys.* 2012;85(10):1–8.
33. Lampert MA, Schilling RB. Chapter 1 Current Injection in Solids: The Regional Approximation Method. In: Willardson RK, Beer ACBT-S and S, editors. *Injection Phenomena*. Elsevier; 1970. p. 1–96.
34. Scott James F. FRS. Magnetoelectric Memories—a Disruptive Techology? *ChemPhysChem.* Wiley-Blackwell; 2009 Jul;10(11):1761–2.

Figure Caption

FIG.1. (a) XRD patterns of Bi_{1-x}Sm_xFeO₃ (x= 0, 0.025, 0.050, 0.075, 0.125, 0.150) samples. * and ^x indicate Bi₂Fe₄O₉ and Bi₂O₃ phases, respectively. (b) Intensity of Bi₂Fe₄O₉ and Bi₂O₃ phases at 2θ = 28°. (c) Weighted Average grain and ferroelectric domain size as a function of Sm-content.

FIG.2. (color online) (a) – (d) Topography, (e)-(h) PFM amplitude, (i) – (l) PFM Phase, and (m) – (p) C-AFM images of Bi_{1-x}Sm_xFeO₃ (x= 0, 0.050, 0.075, and 0.125) samples. For Sm 0 mol% images, the red and white lines outline grains from the topography images with different PFM and C-AFM responses (see main text for details).

For Sm 5 mol% -12.5 mol%, the dash lines simply outline grains from the topography images. All scale bars are 2 μm .

FIG.3. (a) – (c) PFM Phase image of Sm 5% sample taken at $V_{sample}=10$, 0, and -10 V. (d) C-AFM images of the same region at $V_{sample}= 10$ V. The scale bar is 1 μm . (e) Absolute correlation coefficient between the C-AFM at 10 V and the PFM phase images taken at different V_{sample} as a function of Sm content. All scale bars are 2 μm .

FIG.4. (a) I - V curves of ferroelectric domains $\text{Bi}_{1-x}\text{Sm}_x\text{FeO}_3$ ($x = 0 - 0.075$) in semi-logarithmic scale taken with Pt probe. The double logarithmic plot is shown in the inset. The black lines are exponential fits and linear fits, respectively. Slopes of the linear fit are indicated. (b) – (c) ideality factor (β), and offset voltages (V_o) extracted from the I - V curves as a function of Sm content from the I - V curves taken with the Pt and Au probes.

